energies

MDPI

Article

Gain Scheduled Torque Compensation of PMSG-Based Wind Turbine for Frequency Regulation in an Isolated Grid

Haixin Wang [1], Junyou Yang [1,*], Zhe Chen [2], Weichun Ge [3], Shiyan Hu [4], Yiming Ma [1], Yunlu Li [1], Guanfeng Zhang [1] and Lijian Yang [5]

1 School of Electrical Engineering, Shenyang University of Technology, Shenyang 110870, China; sutxny_whx@126.com (H.W.); lnmayiming@126.com (Y.M.); lyl41368@126.com (Y.L.); zguanf@126.com (G.Z.)
2 Department of Energy Technology, Aalborg University, 9100 Aalborg, Denmark; zch@et.aau.dk
3 Liaoning Province Electric Power Company, Shenyang 110006, China; gwc@ln.sgcc.com.cn
4 Department of Electrical and Computer Engineering, Michigan Technological University, Houghton, MI 49931, USA; shiyan@mtu.edu
5 School of Information Science and Engineering, Shenyang University of Technology, Shenyang 110870, China; yanglijian888@163.com
* Correspondence: junyouyang@sut.edu.cn; Tel.: +86-139-4008-8191

Received: 23 May 2018; Accepted: 18 June 2018; Published: 21 June 2018

Abstract: Frequency stability in an isolated grid can be easily impacted by sudden load or wind speed changes. Many frequency regulation techniques are utilized to solve this problem. However, there are only few studies designing torque compensation controllers based on power performances in different Speed Parts. It is a major challenge for a wind turbine generator (WTG) to achieve the satisfactory compensation performance in different Speed Parts. To tackle this challenge, this paper proposes a gain scheduled torque compensation strategy for permanent magnet synchronous generator (PMSG) based wind turbines. Our main idea is to improve the anti-disturbance ability for frequency regulation by compensating torque based on WTG speed Parts. To achieve higher power reserve in each Speed Part, an enhanced deloading method of WTG is proposed. We develop a new small-signal dynamic model through analyzing the steady-state performances of deloaded WTG in the whole range of wind speed. Subsequently, H_∞ theory is leveraged in designing the gain scheduled torque compensation controller to effectively suppress frequency fluctuation. Moreover, since torque compensation brings about untimely power adjustment in over-rated wind speed condition, the conventional speed reference of pitch control system is improved. Our simulation and experimental results demonstrate that the proposed strategy can significantly improve frequency stability and smoothen power fluctuation resulting from wind speed variations. The minimum of frequency deviation with the proposed strategy is improved by up to 0.16 Hz at over-rated wind speed. Our technique can also improve anti-disturbance ability in frequency domain and achieve power balance.

Keywords: deloading method; frequency regulation; gain scheduled compensation; PMSG-based wind turbine; torque control

1. Introduction

At present, wind turbine generators (WTGs) are widely applied. However, its variability and fluctuation increase the difficulty of grid frequency stability and power balance. Especially in an isolated grid, WTGs bring a serious challenge to frequency stability. In addition, sudden load change

may lead to power imbalance. In an isolated grid with a high proportion of wind power penetration, the frequency stability of isolated grid needs to be improved by adjusting WTGs output power [1–4].

WTG needs some power reserves to regulate frequency and balance power [5–9]. WTGs can obtain power reserves mainly in three ways: external energy storage system (ESS), pitch system and converter system [10–14]. Although utilizing many ESS devices can improve frequency stability, there are a few limitations such as the significant increase in economic cost [15]. Therefore, researchers developed model predictive control (MPC) to adjust pitch system for frequency regulation [16]. Some power reserve can be obtained by adjusting the pitch angle to non-zero. However, due to the delay characteristics and a long control period of pitch actuator, pitch system may lead to untimely power adjustment. Therefore, WTGs cannot fully contribute to frequency regulation when relying only on pitch system.

In contrast to ESS and pitch system, converter system has advantages of simple application and fast response to frequency variations [17,18]. Two schemes are commonly used to regulate frequency with converter control. One scheme is that WTG runs with maximum power point tracking (MPPT) control mode, and the power response to frequency variation is achieved by inertia and kinetic energy for a short time [19,20]. The other scheme is that WTG does not track the maximum power point, and the power reserve of WTG is achieved by under-speeding or over-speeding control methods. The work in [21] shows that over-speeding control method is more appropriate to gain power reserves for deloaded WTG. However, at a low wind speed, if frequency regulation is entirely achieved by power reserves of deloaded WTG, the regulation ability is weak, and severe instability may be caused by rapid change of WTG speed. If only inertial characteristic is considered, severe instability may be caused [22]. In terms of frequency regulation method applied to WTG, the most commonly used control strategy is the variable droop control [23]. Wu et al. [24] investigated which droop factor of individual deloaded WTGs can be controlled to improve the primary frequency contribution. Together with [21,25,26], they reach the following consensus. (1) At a low wind speed, there is a possibility of instability when deloaded WTG contributes more energy. Although this could be avoided by limiting the WTG power contribution with a relatively high droop value, the dynamic inertia response capability of WTG cannot be fully utilized; (2) Since utilizing wind speed as a control variable is not appropriate for actual application, variable droop parameters are computed by deloading power and effective droop factor [27]. Despite its effectiveness, the different power compensation capabilities of deloaded WTG in the whole speed range are not considered, which is important.

In summary, the above approaches cannot handle issues such as enhancing power reserve and different power compensation capabilities in each Speed Part. This paper aims to tackle them, through leveraging a new strategy in converter and pitch system for frequency regulation without external ESS. The contributions with respect to the proposed control algorithms are as follows.

- To optimize the primary frequency contribution of WTG, this paper presents a gain scheduled control strategy based on H_∞ theory which combines the advantages of steady-state power reserves and inertia and enhances the torque compensation gain at whole range of wind speed.
- In the deloading method, different deloading factors are designed to smoothen WTG output power and to ensure more power reserve.
- The WTG speed reference of pitch control system is changed to avoid decay or even power oscillation between different Speed Parts caused by torque compensation.
- Comparing with the state-of-the-art MPPT and Droop methods, the frequency deviation with the proposed strategy is reduced by 0.16 Hz and 0.04 Hz, respectively, at over-rated wind speed, and 0.38 Hz and 0.06 Hz, respectively, when wind speed changes.

The rest of the paper is organized as follows. The isolated grid configuration is analyzed in Section 2. An improved deloading torque method of WTG is developed in Section 3. Characteristics of the deloaded WTG with torque compensation are studied in Section 4. Section 5 builds linearized

model and designs H_∞ controller. Simulation and experiment results are shown in Section 6. Finally, the conclusion is given in Section 7.

2. Isolated Grid Configuration

In an isolated grid, load is supplied by a permanent magnet synchronous generator (PMSG) based wind turbine and a diesel generator. The PMSG is connected to the isolated grid by a converter. This work is based on the following wind turbine model in [28]. Some details of this model are included for completeness.

$$\begin{cases} P_m = 0.5\rho C_p(\lambda,\beta)A_r V_w^3, \\ C_p(\lambda,\beta) = c_1(c_2/\lambda_i - c_3\beta - c_4)e^{-c_5/\lambda_i} + c_6\lambda, \\ \frac{1}{\lambda_i} = \frac{1}{\lambda+0.08\beta} - \frac{0.035}{\beta^3+1}, \end{cases} \tag{1}$$

where P_m is mechanical power, ρ is air density, C_p is the power coefficient, λ is the tip speed ratio, β is the pitch angle, A_r is effective area covered by turbine blades, V_w is wind speed, and c_1, c_2, c_3, c_4, c_5 and c_6 are coefficients. The values of relevant parameters in equations and block diagrams of this paper can be seen in Appendix A. The rotor motion equation of PMSG is expressed as:

$$\frac{\mathrm{d}}{\mathrm{d}t}\omega_r = (T_m - T_e)\frac{1}{2H}, \tag{2}$$

where ω_r is the generator angular speed, T_m is mechanical torque, T_e is electric magnetic torque, and H is inertia coefficient. To regulate WTG output power when isolated frequency is unstable, the torque compensation is adopted by Equation (3).

$$T_e = T_{e,del} + T_{e,com}, \tag{3}$$

where T_e is electric magnetic torque, $T_{e,del}$ is deloading torque, and $T_{e,com}$ is torque compensation.

The block diagram of the isolated grid is shown in Figure 1. In the pitch system, τ_β is mechanical time constant of pitch actuator, the classical PI controller is to stabilize the WTG speed at the reference ω_r^*, and the speed reference is changed. P_e is output power of WTG, P_d is diesel generator output power, P_l is load power, and P_{dev} is power deviation. Frequency deviation f_{dev} is obtained by an average aggregate frequency response model $H_g(s)$, while M is inertia coefficient and D is damping coefficient. Diesel generator is controlled to balance power flow [29]. The governor and engine dynamics of diesel generator are modeled as in [23]. T_d and T_g are mechanical time constants of engine and governor, respectively. K_I is an integral coefficient and R is a droop factor. The proposed deloading torque method can be described in Equation (4). $T_{e,com}$ is obtained by the proposed gain scheduled torque compensation strategy.

Frequency regulation strategy depends on load characteristics, and power–frequency regulation of generators can be set by adjusting control systems [30]. Thus, to reduce frequency regulation difficulty and enhance anti-disturbance ability of the isolated grid, WTG is deloaded based on over-speeding control. On the one hand, WTG could adjust output timely according to power demand of isolated grid and reduce pressure of balancing power for diesel generator. On the other hand, WTG output power could be smoothed when wind speed changes. Thus, deloaded WTG has evident advantages for enhancing grid frequency stability.

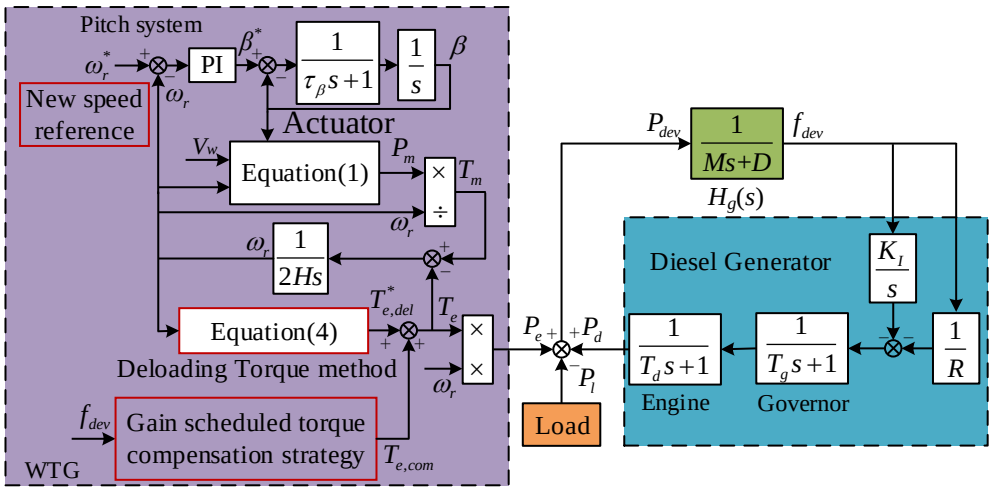

Figure 1. Block diagram of isolated grid.

3. Deloading Method for WTG

Deloading method enables WTG to possess affluent power reserves. Two deloading factors k_{f1} and k_{f2} ($0 < k_{f1} < k_{f2} < 1$) are applied. Corresponding relationships between torque and speed of WTG with deloading factors are shown in Figure 2. The power reserve of WTG can be obtained with deloading factor. The power reserve of WTG increases with decreasing deloading factor. It can be seen that the power reserve with k_{f2} is between those with k_{f1} and MPPT. The capacity of power reserve of WTG depends on the selection of deloading factors. When wind speed is higher than its rated value, k_{f2} is selected as 0.9 to obtain 0.1 pu power reserve of WTG. If k_{f1} is selected, higher power reserves can be presented but causes more wind energy loss. When wind speed is lower than its rated value, k_{f2} may not be able to provide WTG sufficient power reserve to regulate frequency. Therefore, k_{f1} may be selected as 0.8 to possess more power reserve for WTG to regulate frequency. The deloading factors may vary theoretically from 1 (no power reserve) to 0 (total curtailment). The selection of deloading factors is related to capacity of a WTG and power requirement of grid [31].

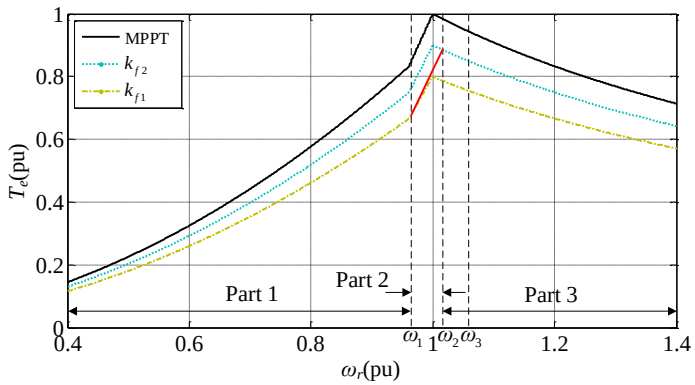

Figure 2. The torque curves of WTG with different deloading factors.

To obtain appropriate power reserve in each Speed Part and expand speed range in Part 2, three Speed Parts are defined as follows.

Part 1: $\omega_0 < \omega_r \leq \omega_1$. In this Part, to provide WTG more power reserves, k_{f1} is selected. ω_0 is the cut-in angular speed and ω_1 is the initial angular speed.

Part 2: $\omega_1 < \omega_r < \omega_2, (\omega_2 > \omega_{r,\mathrm{nom}})$. This Part is the transition of Parts 1 and 3. $\omega_{r,\mathrm{nom}}$ is the rated speed of WTG. The electromagnetic torque reference is proportional to WTG speed, and the red

transition curve as shown in Figure 2 is applied for smoothening its output power. The purpose of expanding speed range is to reduce power variation when wind speed changes.

Part 3: $\omega_2 \leq \omega_r < \omega_{r,\max}$. k_{f2} is chosen in this Part. WTG output power is the highest among all Parts. The power reserve in this Part is also the largest. $\omega_{r,\max}$ is the speed up limit. When WTG speed decreases, more energy would be obtained by adjusting pitch angle, and WTG speed reference of pitch control system is changed to be ω_2 naturally.

Based on the above description, an improved torque control method is proposed to ensure more reserve. The red transition curve as shown in Figure 2 is adopted in Part 2. The proposed deloading torque in this paper is expressed by Equation (4).

$$T_{e,del} = \begin{cases} k_{f1} k_{opt} \omega_r^2, & \omega_0 < \omega_r \leq \omega_1 \\ \frac{k_{f2} \frac{P_{e,\text{nom}}}{\omega_2} - k_{f1} k_{opt} \omega_1^2}{\omega_2 - \omega_1} (\omega_r - \omega_2) + k_{f2} \frac{P_{e,\text{nom}}}{\omega_2}, & \omega_1 < \omega_r < \omega_2 \\ k_{f2} \frac{P_{e,\text{nom}}}{\omega_r}, & \omega_2 \leq \omega_r < \omega_{r,\max} \end{cases} \tag{4}$$

where k_{opt} is the optimal factor, and $P_{e,\text{nom}}$ is the rated power. Furthermore, steady-state simulation is conducted with k_{f1} and k_{f2}. The relationship between power and speed is obtained as shown in Figure 3. The shaded part is the area of adjustable power of deloaded WTG for frequency regulation.

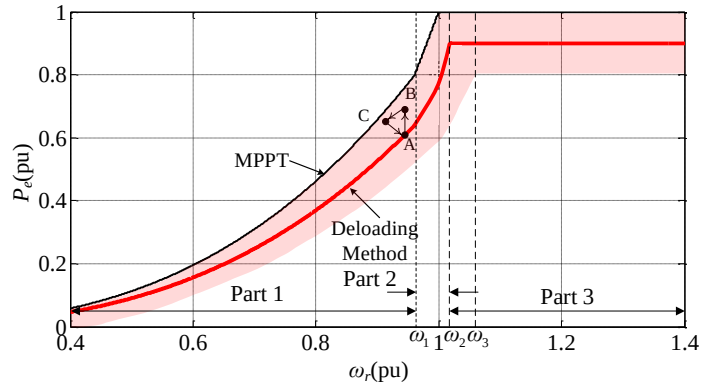

Figure 3. The output power of deloaded WTG.

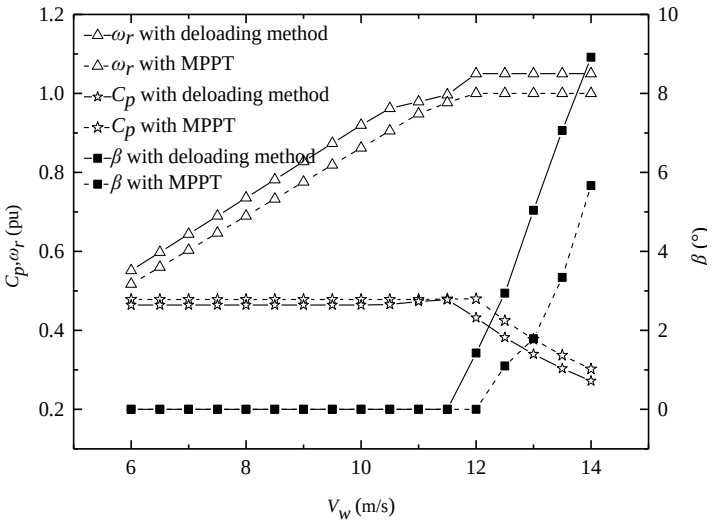

Figure 4. Control laws of the deloaded WTG.

Control laws of the proposed deloading method are further analyzed by steady-state simulation. Simulation results in the whole range of wind speed are shown in Figure 4. When wind speed approaches the rated value, WTG with deloading method would reach the rated angular speed. Thus, the action of pitch angle with deloading method is earlier than that with MPPT control. Correspondingly, C_p with deloading method is also smaller than the value with MPPT control. In other words, the rated wind speed of deloaded WTG is derated by keeping certain power reserve.

4. Analysis of Deloaded WTG

At under-rated wind speed, the deloaded WTG operates at Point A in Figure 3, and certain power reserve of WTG is obtained. When frequency drops, WTG increases output power to isolated grid. Due to rapid change of increasing output power, WTG's operation point moves to Point B. Furthermore, increasing output power of WTG leads to overload; thus, its speed decreases, and WTG's operation point moves to Point C. When frequency deviation becomes stable at almost zero or within the dead band, the WTG will return to Point A. However, at over-rated wind speed, the deloaded WTG operates at speed ω_2. When isolated grid requires power, the deloaded WTG would increase torque to supply power by torque compensation controller. Since adjustment of pitch angle is not timely, the WTG speed would be decreased from speed ω_2, which leads to decrease of $T_{e,del}$ of deloading torque controller. At this point, WTG speed is influenced by torque compensation controller, pitch controller and deloading torque controller. Speed decreasing leads to deloading torque reduction and untimely power adjustment. Since untimely power adjustment can be induced, angular speed reference ω_2 of pitch control system is not suitable when WTG participates in frequency regulation. However, when torque compensation component of WTG is added to support frequency, with a reasonable and higher speed reference ω_3 of pitch control system, pitch angle would begin operation timely, and more power can be absorbed by wind turbine. Thus, this paper adopts ω_3 ($\omega_3 > \omega_2$) as a new speed reference of pitch control system to avoid decay or even power oscillation caused by torque compensation. ω_3 is designed in pitch control system. This new speed reference increases adjustment range of WTG speed and regulation time for pitch system. The selection of ω_2 and ω_3 is related to capacity and inertia of WTG. The selection purpose of ω_2 is to expand speed range for reducing power variation when wind speed changes. The selection purpose of ω_3 is to ensure regulating power effectively and extend regulation time for pitch control system response.

Simulation above rated wind speed is performed, and results are shown in Figure 5. ω_2 and ω_3 are set at 1.02 pu and 1.05 pu, respectively. Torque compensation demand is added by 0.06 pu. With traditional deloading method in [23,26], deloaded WTG increases output power to 0.96 pu rapidly. However, when a constant torque compensation component demand 0.06 pu is added, the rotational speed is decreased from angular speed reference ω_2, which leads to decreases of T_e and P_e. In this period, speed decreasing leads to deloading torque decreasing and power drops. When deloading method in Equation (4) with ω_2 is applied, the output power is also not adequate. When deloading method in Equation (4) with ω_3 is applied, a higher rotational speed with a reasonable torque creates a higher power. Deloaded WTG increases output power to 0.96 pu rapidly, and some speed jitter is caused by torque compensation. Simulation results show the necessity of resetting speed reference of pitch control system.

Moreover, steady-state performances of the deloaded WTG are simulated at different wind speeds. The steady-state simulation results are shown in Tables 1 and 2. In Table 1, wind speed is set at 10 m/s, and WTG is deloaded by Equation (4). Torque and power of WTG increase with the increasing torque compensation component $T_{e,com}$, and then corresponding speed of WTG decreases. In Table 2, wind speed is set at 13.5 m/s, and WTG speed is adjusted at 1.05 pu of its rated speed by pitch control. It can be seen that the greater the absolute value of $T_{e,com}$ is, the more output power P_e can be compensated. The steady-state power reserve in Part 1 is less than that in Part 3, and the inertial characteristic would be utilized to possess more available power reserve in Part 1 for short-time frequency regulation.

The gap of power reserve between different Speed Parts is narrowed, which states the rationality of using different reasonable deloading factors based on Speed Parts.

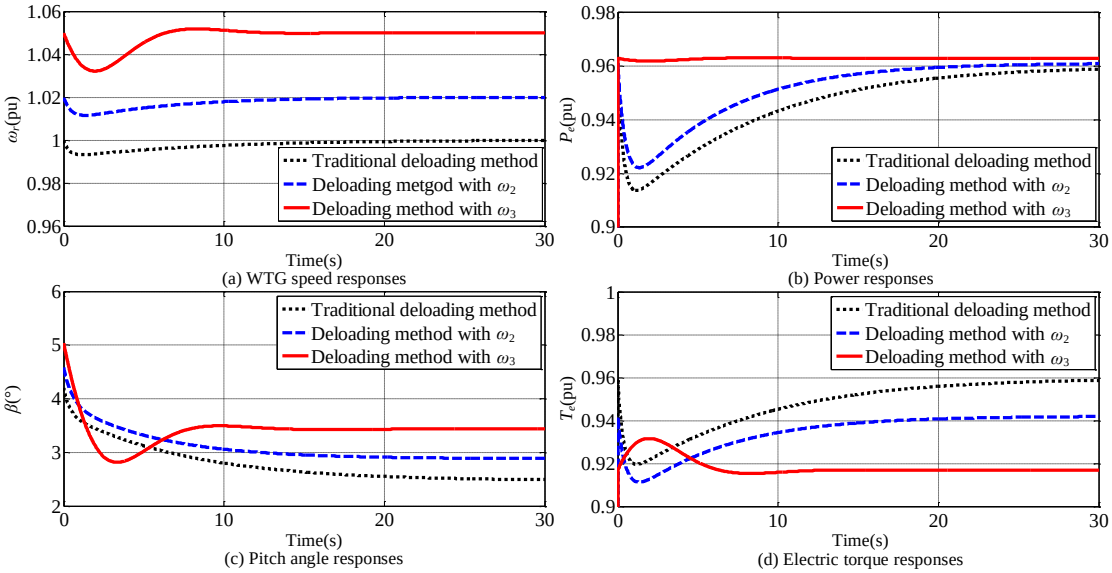

Figure 5. Different responses of deloaded WTG.

Table 1. Output Characteristics of the Deloaded WTG at 10 m/s.

$T_{e,com}$ (pu)	ω_r (pu)	T_e (pu)	P_e (pu)	Power Reserve (pu)
−0.2	0.9737	0.5443	0.5299	0~0.0488
−0.1	0.9591	0.5623	0.5393	−0.0094~0.0394
0	0.9195	0.6088	0.5598	−0.0299~0.0189
0.1	0.8772	0.654	0.5737	−0.0438~0.005
0.2	0.8306	0.6967	0.5787	−0.0488~0

Table 2. Output Characteristics of the Deloaded WTG at 13.5 m/s.

$T_{e,com}$ (pu)	ω_r (pu)	T_e (pu)	P_e (pu)	Power Reserve (pu)
−0.2	1.05	0.6571	0.7	0~0.3
−0.1	1.05	0.7571	0.795	−0.095~0.205
0	1.05	0.8571	0.9	−0.2~0.1
0.1	1.05	0.9571	1	−0.3~0

5. Design of Torque Compensation Controller

5.1. Linearized Models of the Deloaded WTG

According to the motion equation and mechanical power of WTG in [28], linearized equation can be expressed by Equation (5).

$$\begin{cases} \Delta P_m - \Delta P_e = H\omega_{r0}\frac{\mathrm{d}\Delta\omega_r}{\mathrm{d}t}, \\ \Delta P_m = a_1\Delta\beta + a_2\Delta\omega_r + a_3\Delta V_w, \end{cases} \tag{5}$$

where "Δ" indicates a small-signal value around the operating point, subscript "0" indicates steady-state value around the operating point, and a_1, a_2 and a_3 depending on the variables at stable operating point are calculated by Equation (6) [32].

$$\begin{cases} a_1 = \frac{\partial P_m}{\partial \beta} = 0.5\rho A_r V_{w0}^3 \frac{\partial C_p}{\partial \beta}, \\ a_2 = \frac{\partial P_m}{\partial \omega_r} = 0.5\rho A_r V_{w0}^3 \frac{\partial C_p}{\partial \lambda} \frac{\partial \lambda}{\partial \omega_r}, \\ a_3 = \frac{\partial P_m}{\partial V_w} = 0.5\rho A_r (3C_{p0} V_{w0}^2 + V_{w0}^3 \frac{\partial C_p}{\partial \lambda} \frac{\partial \lambda}{\partial V_w}). \end{cases} \tag{6}$$

According to Equations (4)–(6), linearized models of deloaded WTG can be written as

$$\Delta\dot{\omega}_r = \begin{cases} \frac{a_1\Delta\beta + (a_2 - 3k_{f1}k_{opt}\omega_{r0}^2 - T_{e,com0})\Delta\omega_r + a_3\Delta V_w - \omega_{r0}\Delta T_{e,com}}{H\omega_{r0}}, & \omega_0 < \omega_r \le \omega_1 \\ \frac{a_1\Delta\beta + [a_2 - \frac{k_{f2}\frac{P_{e,\mathrm{nom}}}{\omega_2} - k_{f1}k_{opt}\omega_1^2}{\omega_2 - \omega_1}(2\omega_{r0} - \omega_2) - k_{f2}\frac{P_{e,\mathrm{nom}}}{\omega_2} - T_{e,com0}]\Delta\omega_r + a_3\Delta V_w - \omega_{r0}\Delta T_{e,com}}{H\omega_{r0}}, & \omega_1 < \omega_r < \omega_2 \\ \frac{a_1\Delta\beta + (a_2 - T_{e,com0})\Delta\omega_r + a_3\Delta V_w - \omega_{r0}\Delta T_{e,com}}{H\omega_{r0}}, & \omega_r \ge \omega_2. \end{cases} \tag{7}$$

The linearized models take deloading factors and torque compensation value into account. In Parts 1 and 2, k_{f1} and k_{f2} are introduced, WTG speed is mainly affected by wind speed and torque compensation. In Part 3, the output power is constant without power compensation, and a_1, a_2, a_3 and relevant variables are related to k_{f2}. Pitch angle needs to be considered, and the linearized model of pitch control system as [33]:

$$\begin{cases} \Delta\beta^* = (K_{\beta p} + K_{\beta i}/s)\Delta\omega_r, \\ \Delta\beta = \frac{1}{\tau_\beta s + 1}\Delta\beta^*, \end{cases} \tag{8}$$

where $K_{\beta p}$ and $K_{\beta i}$ are proportional and integral coefficients.

Based on the above analysis, the linearized models in Parts 1 and 2 could not reflect operation characteristics in Part 3. Therefore, it is necessary to study compensation ability of deloaded WTG in different Speed Parts. Considering the complexity and small speed range of the dynamic model in Part 2, one torque compensation controller is commonly applied to Parts 1 and 2, another one is adopted in Part 3.

5.2. Design of Gain Scheduled Torque Compensation Controller

The purpose of torque compensation controller is to complement power shortage and ensure stable operation of WTG. H_∞ control can overcome the influences of wind speed or sudden load changes, and achieve optimal operation of WTG [34,35]. Thus, H_∞ controller is more suitable for frequency regulation in the deloaded WTG. The overall block diagram of H_∞ control is shown in Figure 6. Specific designs of the controller are as follows.

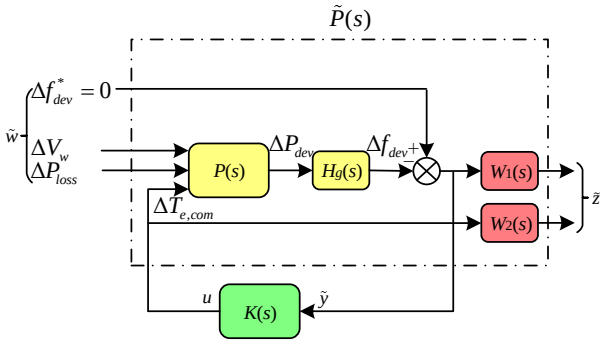

Figure 6. Block diagram of H_∞ control.

According to linearized models in Equation (8), $[x_1\ x_2]^{\mathrm{T}}$ are chosen as state variables. Small-signal of WTG speed $\Delta\omega_r$ is added to the state variables $x = [x_1\ x_2\ \Delta\omega_r]^{\mathrm{T}}$. The external input is $w = [\Delta V_w\ \Delta P_{loss}]^{\mathrm{T}}$. P_{loss} is the sum of P_d and P_l. The input signal is $u = \Delta T_{e,com}$. The output signal of plant P tracks deviation $\Delta P_{dev} = \Delta P_e - \Delta P_{loss}$. The plant P is described by state equation:

$$\dot{x} = A_1 x + B_{11} w + B_{12} u \tag{9}$$

with $A_1 = \begin{bmatrix} -\frac{1}{\tau_\beta} & 0 & 1 \\ 1 & 0 & 0 \\ \frac{a_1 q_1}{H\omega_{r0}} & \frac{a_1 q_2}{H\omega_{r0}} & \frac{a_2 - q_3}{H\omega_{r0}} \end{bmatrix}$, $B_{11} = \begin{bmatrix} 0 & 0 \\ 0 & 0 \\ \frac{a_3}{H\omega_{r0}} & 0 \end{bmatrix}$, $B_{12} = \begin{bmatrix} 0 \\ 0 \\ -\frac{1}{H} \end{bmatrix}$, and output equation:

$$y = C_1 x + D_{11} w + D_{12} u, \tag{10}$$

with $C_1 = \begin{bmatrix} 0 & 0 & q_3 \end{bmatrix}$, $D_{11} = \begin{bmatrix} 0 & -1 \end{bmatrix}$, $D_{12} = \omega_{r0}$, where $q_1 = \frac{K_{\beta p}}{\tau_\beta}$, $q_2 = \frac{K_{\beta i}}{\tau_\beta}$, $q_3 = \begin{cases} 3k_{f1}k_{opt}\omega_{r0}^2 + T_{e,com0}, & \text{Parts } 1,2 \\ T_{e,com0}, & \text{Part } 3 \end{cases}$.

Subsequently, the corresponding plant transfer function is:

$$P = \begin{bmatrix} A_1 & B_{11} & B_{12} \\ C_1 & D_{11} & D_{12} \end{bmatrix}. \tag{11}$$

In Figure 6, $H_g(s)$ is given by Equation (12).

$$H_g = \begin{bmatrix} A_g & B_g \\ C_g & D_g \end{bmatrix}, \tag{12}$$

where $A_g = -D/M$, $B_g = 1$, $C_g = 1/M$, and $D_g = 0$. Weighting function $W_2(s)$ is chosen as $W_2(s) = \mu$, and weighting function $W_1(s)$ is chosen as:

$$W_1 = \begin{bmatrix} A_2 & B_2 \\ C_2 & D_2 \end{bmatrix}. \tag{13}$$

Thus, frequency regulation issues for the deloaded WTG are transferred into H_∞ norm minimization of the transfer function $T_{\widetilde{z}\widetilde{w}}$ from input $\widetilde{w} = \begin{bmatrix} \Delta f_{dev}^* & \Delta V_w & \Delta P_{loss} \end{bmatrix}^{\mathrm{T}}$ to output signal $\widetilde{z} = \begin{bmatrix} z_1 & z_2 \end{bmatrix}^{\mathrm{T}}$. The closed loop system is expressed as:

$$\begin{bmatrix} \widetilde{z} \\ \widetilde{y} \end{bmatrix} = \widetilde{P} \begin{bmatrix} \widetilde{w} \\ u \end{bmatrix}, \tag{14}$$

where $\widetilde{P}$ of the system transfer function can be expressed as:

$$\widetilde{P} = \begin{bmatrix} A_1 & \boldsymbol{O} & \boldsymbol{O} & \boldsymbol{O} & B_{11} & B_{12} \\ B_g C_1 & A_g & 0 & 0 & B_g D_{11} & B_g D_{12} \\ -B_2 D_g C_1 & -B_2 C_g & A_2 & B_2 & -B_2 D_g D_{11} & -B_2 D_g D_{12} \\ -D_2 D_g C_1 & -D_2 C_g & C_2 & D_2 & -D_2 D_g D_{11} & -D_2 D_g D_{12} \\ \boldsymbol{O} & 0 & 0 & 0 & 0 & \mu \\ -D_g C_1 & -C_g & 0 & 1 & -D_g D_{11} & -D_g D_{12} \end{bmatrix}. \tag{15}$$

$W_1(s)$ is a tracking performance weighting function of frequency deviation. To improve the sensitivity of frequency deviation response, $W_1(s)$ has the characteristics of high gain and low pass.

$W_2(s)$ is the upper bound of the uncertainty for model parameters. $W_1(s)$ and $W_2(s)$ are designed by testing repeatedly in this paper as follows:

$$\begin{cases} W_1(s) = \frac{4.2}{s+100}, W_2(s) = 0.03 \quad \text{(Parts 1, 2)} \\ W_1(s) = \frac{1.4}{s+100}, W_2(s) = 0.03 \quad \text{(Part 3)}. \end{cases} \tag{16}$$

According to the augmented matrix $\widetilde{P}$, $K_1(s)$ and $K_2(s)$ are obtained by using a MATLAB (7.13) function *hinfsyn* and reduced as:

$$\begin{cases} K_1(s) = \frac{9002s^2+1.093\times10^6 s+1.931\times10^7}{s^3+2.021\times10^4 s^2+4.119\times10^6 s+2.109\times10^8}, \\ K_2(s) = \frac{1097s^2+1.097\times10^5 s+421.2}{s^3+1.424\times10^4 s^2+1.414\times10^6 s+5429}. \end{cases} \tag{17}$$

The $K_1(s)$ has a steady-state gain of 0.0916, two zeros at -21.4599 and -99.9576, and three poles at -101, -104 and -2×10^4. $K_1(s)$ is simplified to $K_1(s) = 0.0916(s + 21.4599)/(s + 104)$. The $K_2(s)$ has a steady-state gain of 0.0776, two zeros at -0.0038 and -100, and three poles at -0.00384, -100 and $-14{,}140$. Subsequently, $K_2(s)$ is simplified to $K_2(s) = 0.0776/(s + \mathrm{p})$, where p is a sufficiently large pole.

The purposes of gain scheduled torque compensation controller are to improve anti-disturbance ability for frequency and ensure power balance. The proposed H_∞ control has mainly two merits as follows: (1) Different power reserves in each Speed Part are considered in the piecewise controller. In this way, the proposed strategy could support power shortage based on frequency deviation and WTG Speed Part. If the same gain is applied, the generated power compensation in Part 3 is more than that in Parts 1 and 2. To improve the frequency regulation ability in Parts 1 and 2, the steady-state gain of $K_1(s)$ is bigger than that of $K_2(s)$; (2) The H_∞ controller has another advantage of making full use of power reserve and inertia characteristic for frequency regulation. In Parts 1 and 2, the power compensation of WTG is mainly dependent on less power reserve and inertial characteristic for a short time. When the frequency change behavior is slow, it is not suitable to use the inertia characteristic for a long time. The overload and instability of WTG are easily induced, and the gain of $K_1(s)$ is required to be smaller. When the frequency change is more rapid, it is available to use the inertia characteristic. Here, the gain of $K_1(s)$ is expected to be bigger. The power reserve in Part 3 is larger and constant. Thus, the gain of $K_2(s)$ is almost constant at low frequency and attenuates rapidly for noise immunity in higher frequencies. $K_1(s)$ and $K_2(s)$ are consistent with the expected design. It is also clear that the anti-disturbance ability in Part 3 is stronger than that in Parts 1 and 2.

6. Simulation and Experiment

6.1. Simulation Setup

To verify the effectiveness and validity of the proposed H_∞ controller, it is compared with MPPT controller and variable droop controller (Droop for short) in simulation and experiment. H_∞ controller and Droop controller are based on the deloading method in Equation (4). Droop controller is introduced in Equation (18) [23]. Parameters of isolated grid are shown in Table 3.

$$T_e = T_{e,del} + K_P(f_{rated} - f), \tag{18}$$

where K_P is variable droop factor, and f_{rated} is the rated frequency of isolated grid. When K_P is small, frequency regulation ability of WTG will be weakened. When K_P is great, unreasonable torque compensation component may worsen system stability.

Table 3. Parameters of Isolated Grid.

System	Parameters	Values
Diesel generator	Rated power	10 kW
-	Rated voltage	400 V
-	Rated frequency	50 Hz
Constant load	Rated power	5.5 kW
Electronic load	Rated power	10 kW
Wind turbine	Rated speed	12 m/s
PMSG	Rated power	10 kW

6.2. Simulation Results

To compare the effectiveness of the presented strategy when load changes, simulation is conducted. Simulation period is 10 s, and wind speeds are set as constants. At the instant of 4 s, load demand is increased by 1.5 kW. The simulation results are shown in Figures 7 and 8.

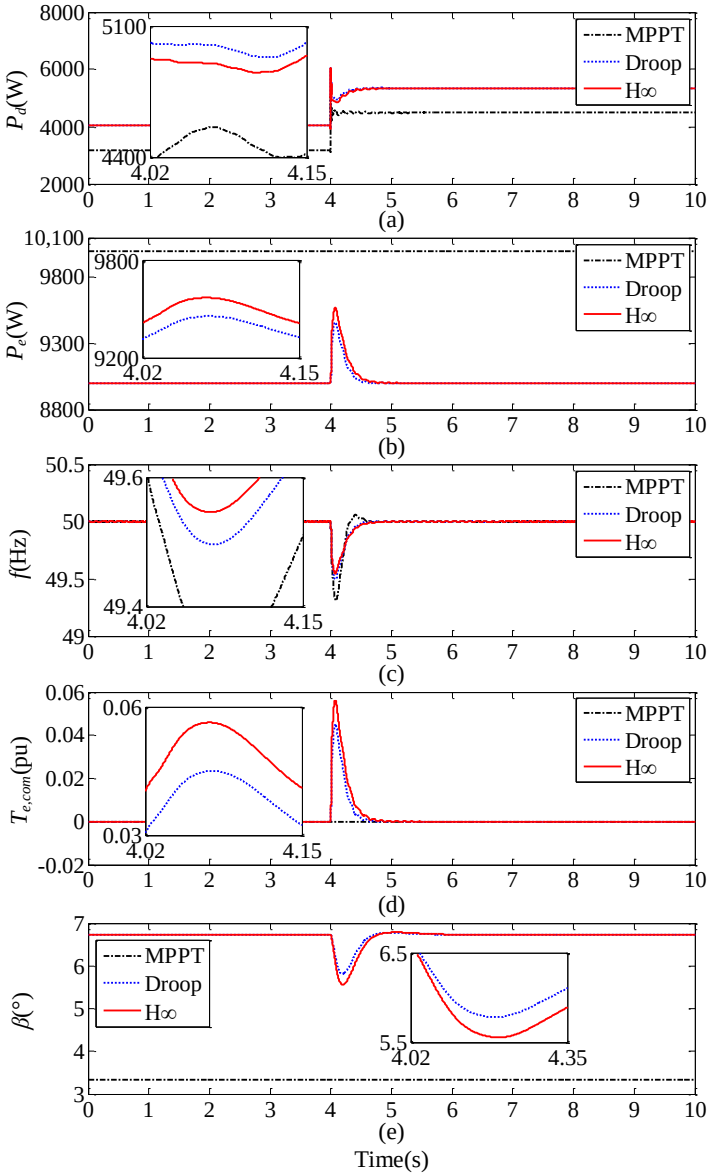

Figure 7. Simulation results when V_w is 13.5 m/s. (**a**) output power of diesel generator; (**b**) output power of WTG; (**c**) isolated grid frequency; (**d**) torque compensation component; (**e**) pitch angle.

6.2.1. Case 1: At Over-Rated Wind Speed

Wind speed is set to 13.5 m/s. In Figure 7a, due to lack of wind power contribution, P_d with MPPT control is less than those with deloading method. From 4.02 s to 4.15 s, P_d with H_∞ control is 100 W which is less than that with Droop control. The variation of P_d is smoothened by power reserve of deloaded WTG, the more WTG output power is, means that the less P_d is. As shown in Figure 7b, P_e with MPPT is constant and the power reserve with deloading method is 1 kW for regulating frequency. Compared with Droop control, the power compensation is increased up to 120 W with H_∞ control. The frequency curves are shown in Figure 7c. With MPPT control, the frequency drops to 49.31 Hz when load is increased. The frequency variation with H_∞ control is the smallest. The torque compensation responses to frequency deviation are shown in Figure 7d. In this case, controller $K_2(s)$ is applied, the maximum possible torque compensation is 0.1 pu. When frequency drops rapidly, due to the use of inertia characteristic and power reserve, the peak torque compensation value with H_∞ control is 0.057 pu. The peak torque compensation value with Droop control is 0.045 pu. The torque compensation of H_∞ control is up to 1.27 times of that of Droop control. It can be seen that the torque compensation gain of H_∞ control is higher than Droop control. The pitch angle curves of WTG with different methods are shown in Figure 7e. At a same over-rated wind speed, since the obtained wind power with deloading method is always less than its rated value, the pitch angles with deloading method are 6.7° bigger than that (3.4°) with MPPT control. When the deloaded WTG increases output power to regulate frequency, more energy is obtained by adjustment of pitch angle.

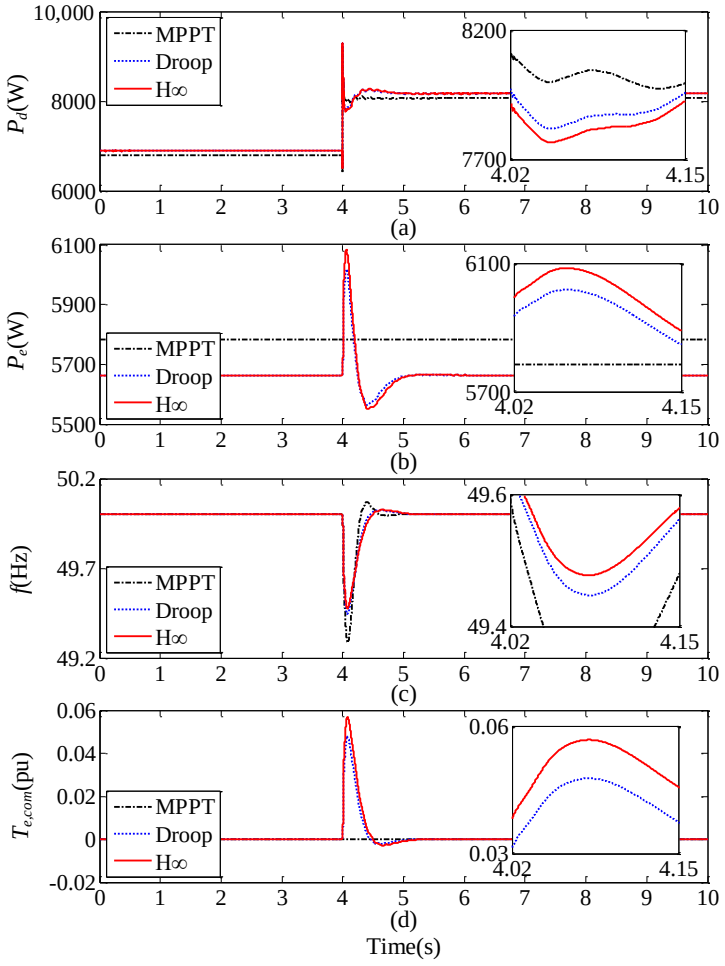

Figure 8. Simulation results when V_w is 10 m/s. (**a**) output power of diesel generator; (**b**) output power of WTG; (**c**) isolated grid frequency; (**d**) torque compensation component.

6.2.2. Case 2: At Under-Rated Wind Speed

Wind speed is set to 10 m/s. In Figure 8a, when load demand is increased at 4 s, P_d is lowered. Meantime, the WTG with deloading method participates in balancing power. Due to the WTG's power contribution since 4 s, compared to MPPT control, diesel generator outputs with deloading methods are reduced. In Figure 8b, the initial outputs of WTG with MPPT and deloading method are 5.79 kW and 5.66 kW, respectively, and the steady-state power reserve of deloaded WTG is 130 W. When load increases, the instantaneous power compensation of WTG with H_∞ control is about 400 W which is larger than that (340 W) with Droop control. Due to the inertia characteristic, the power compensations of deloaded WTG are more than the steady-state power reserve of 130 W. The frequency curves are shown in Figure 8c. When the frequency is disturbed by a load change at 4 s, the frequency variation with H_∞ control is the smallest. In Figure 8d, $T_{e,com}$ with Droop control is weaker than that with H_∞ control. The torque compensation response gain is enhanced by H_∞ control.

6.3. Experimental Setup

Experimental platform is shown in Figure 9. The platform in laboratory contains diesel generator, constant load, electronic load, indoor WTG and RTLAB real-time simulator. The task of diesel generator is to support voltage and frequency. The constant load is utilized to imitate conventional load. The load change is realized by the electronic load. The indoor WTG is simulated by operating cabinet, grid connected cabinet, main control cabinet, motor and PMSG. The driving system of wind turbine simulation is composed of inverter and motor. The output power of motor is adjusted by inverter. The wind turbine simulation algorithm is applied to PLC. According to wind speed, pitch angle and real-time generator speed, wind turbine mechanical power is calculated by Equation (1). Wind speed is obtained by look-up table or external input. The pitch angle control system is also simulated in PLC, and its specific strategy is included in Figure 1. In this way, the mechanical torque is calculated. WTG speed reference is obtained by Equation (1) which is sent to the inverter. PMSG is driven by the motor. Subsequently, the generated power is output to the isolated grid through the converter. The simulation of indoor WTG is implemented. Voltage signals of isolated grid are transmitted to RTLAB real-time simulator for calculating frequency. Torque compensation controllers are programmed in the RTLAB. Torque compensation component is sent to the PLC through analog interfaces. The operation condition of isolated grid is monitored by HMI. The key data are recorded by measurement instrument.

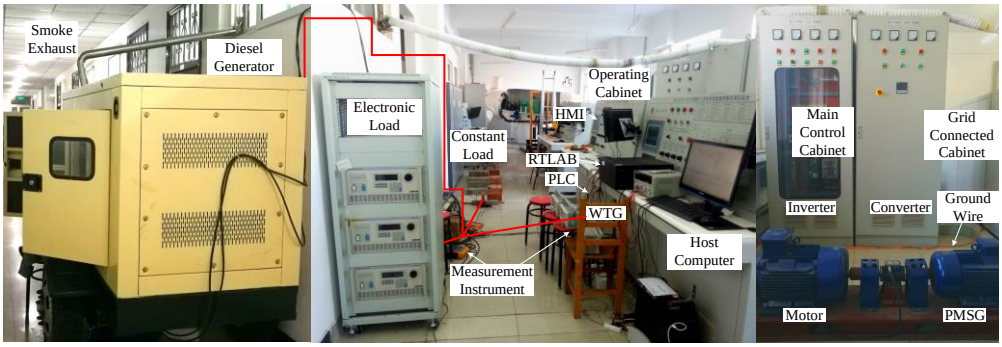

Figure 9. Experimental platform.

The dead zone of frequency regulation is set at 0.18 Hz. When frequency deviation is outside the dead zone, the signal of torque compensation component is enabled. Once frequency deviation inside the dead zone, the present compensation component is held in the compensation controller. To verify the effectiveness of the proposed strategy, experiments for different cases were carried out.

6.4. Experimental Results

6.4.1. Case 1: At Over-Rated Wind Speed

Wind speed is set at 13.5 m/s, load demand is added by 1.5 kW at 4 s, and experimental period is 10 s. Experimental results with different control methods are shown in Figure 10a,b. When MPPT control is adopted, at 4 s, since the load is increased, frequency deviation of isolated grid dips to −0.64 Hz. WTG output power is 10 kW, and its torque is constant. With Droop control, initial output power of deloaded WTG is 9 kW. The output power of deloaded WTG is increased by Droop control according to frequency deviation. The output power of WTG is up to 9.34 kW, and the minimum frequency deviation is −0.52 Hz. With H_∞ control, the maximum output power is about 9.40 kW, the minimum frequency deviation is −0.48 Hz. It can be seen that the variation of frequency deviation with H_∞ control is smaller than the other control methods.

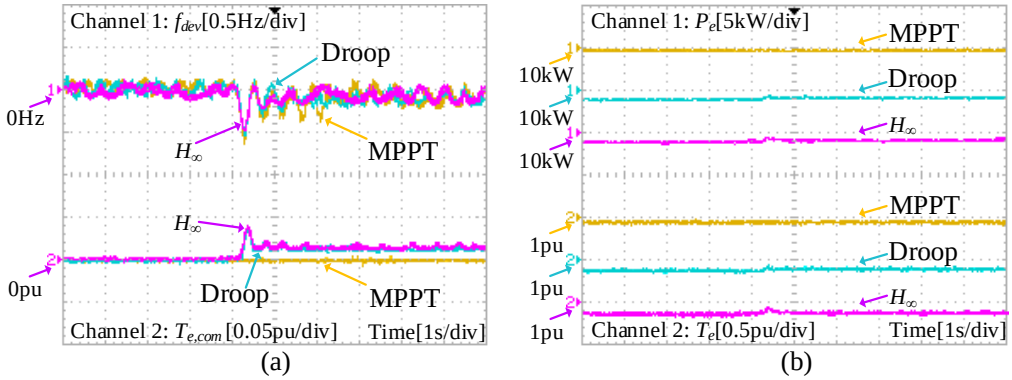

Figure 10. Experimental results when V_w is 13.5 m/s.

6.4.2. Case 2: At Under-Rated Wind Speed

Wind speed is set to 10 m/s, load demand is added by 1.5 kW at 4 s, and the experimental results with different control methods are shown in Figure 10a,b. The WTG output power with MPPT control is 5.7 kW. When load is increased, the frequency deviation dips to −0.66 Hz. With Droop control, the output power of WTG is compensated by 0.2 kW, and the minimum of frequency deviation is reduced to −0.6 Hz. With the proposed H_∞ control, frequency deviation variation is suppressed, and restores to dead zone. The maximum power compensation of WTG is nearby 0.3 kW, the minimum frequency deviation is −0.56 Hz. It can be seen that the frequency regulation capability is further enhanced by H_∞ control.

6.4.3. Summary of Results

To quantify the comparison between the MPPT, droop and H_∞ control algorithms for simulations and experiments, the important values are shown in Table 4. $P_{e,com\max}$ indicates the maximum of power compensation of WTG. The minimum of frequency deviation $f_{dev,\min}$ is also shown. It can be seen that, at different cases, $P_{e,com\max}$ with H_∞ control is larger than those with the other control methods, and $f_{dev,\min}$ with H_∞ control is the largest. The power compensations of WTG at over-rated wind speed is larger than that those at under-rated speed. With MPPT control, WTG has no power compensation. At over-rated wind speed, comparing the other methods, the minimum of frequency deviation with H_∞ control is enhanced by 0.16 Hz and 0.04 Hz, respectively. The primary frequency regulation contribution of WTG is further enhanced by H_∞ control. Compared with simulation results, there are oscillations in the experimental results. The oscillations could be caused by the weak mechanical system of diesel generator. In addition, according to the simulation and experimental curves shown in Figures 7, 8, 10 and 11, the overall trend is consistent.

Table 4. Comparison with different control methods in simulation and experiment.

Control Strategy		MPPT Control	Droop Control	H_∞ Control
Simulation	Case 1, $P_{e,com\max}$	0	450 W	570 W
	Case 1, $f_{dev,\min}$	−0.69 Hz	−0.5 Hz	−0.45 Hz
	Case 2, $P_{e,com\max}$	0	354 W	420 W
	Case 2, $f_{dev,\min}$	−0.71 Hz	−0.55 Hz	−0.52 Hz
Experiment	Case 1, $P_{e,com\max}$	0	340 W	400 W
	Case 1, $f_{dev,\min}$	−0.64 Hz	−0.52 Hz	−0.48 Hz
	Case 2, $P_{e,com\max}$	0	200 W	300 W
	Case 2, $f_{dev,\min}$	−0.66 Hz	−0.6 Hz	−0.56 Hz

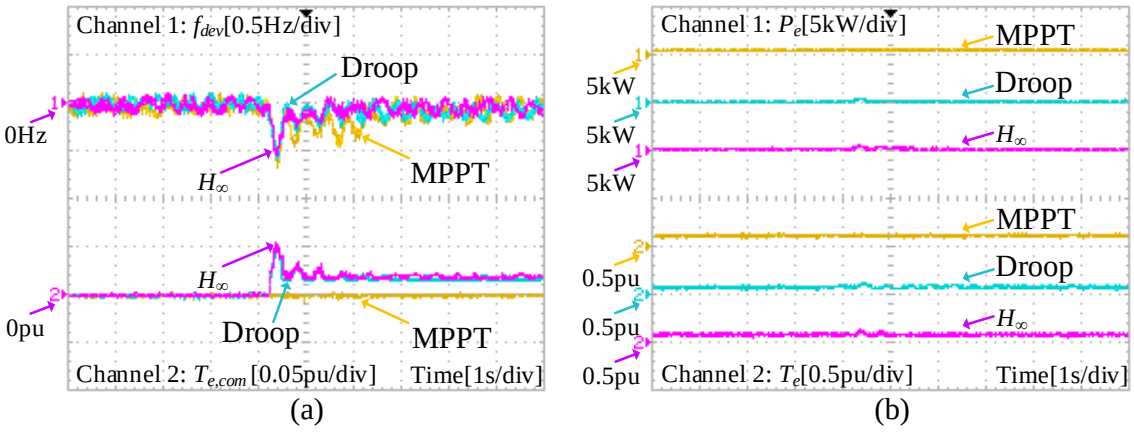

Figure 11. Experimental results when V_w is 10 m/s.

6.4.4. Case 3: Wind Speed Change

In this case, wind speed is variable, as shown in Figure 12; load capacity is constant; and experimental period is 100 s. Wind speed change leads to output power variation of WTG. To suppress frequency fluctuation caused by WTG output power, deloaded WTG provides power compensation to isolated grid when wind speed changes. Experimental results are shown in Figure 13a,b. When MPPT control is applied, WTG has no power compensation, the minimum P_e is 6.2 kW, and the minimum frequency deviation is −0.9 Hz. When Droop control is adopted, the minimum P_e is 6.0 kW, and the minimum frequency deviation is −0.58 Hz. With the proposed H_∞ control, change of P_e is smaller than those with other control methods. The minimum P_e is 6.2 kW, and the minimum frequency deviation is reduced to −0.52 Hz. The torque compensation controller provides a damping to the power variation of WTG. The capability of torque compensation with H_∞ control is stronger than that with droop control. The change of frequency with H_∞ control is the smallest. The pitch angle curves are shown in Figure 13b. At over-rated speed, the pitch angles with deloading method are greater than that with MPPT control. At under-rated speed, the pitch angles go to zero to obtain the maximum wind energy. Due to the delay characteristic of pitch control system, the pitch angle curve with H_∞ control is roughly the same as the curve with Droop control. The specific data comparison is shown in Table 5. Comparing the other methods, the minimum of frequency with H_∞ control is enhanced by 0.38 Hz and 0.06 Hz, respectively, which shows that the H_∞ control enhances the ability of WTG to suppress frequency variation.

Table 5. Comparison with different control methods when wind speed changes.

Control Strategy	MPPT Control	Droop Control	H_∞ Control
Maximum of P_e	10 kW	9 kW	9 kW
Minimum of P_e	6.2 kW	6.0 kW	6.2 kW
Maximum of f_{dev}	0.2 Hz	0.1 Hz	0.1 Hz
Minimum of f_{dev}	−0.9 Hz	−0.58 Hz	−0.52 Hz

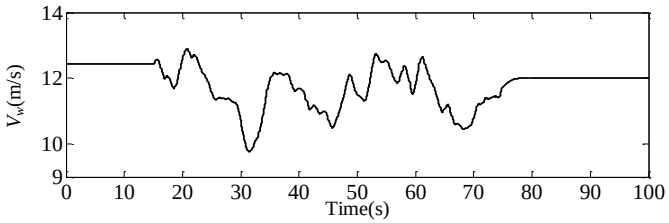

Figure 12. Wind speed.

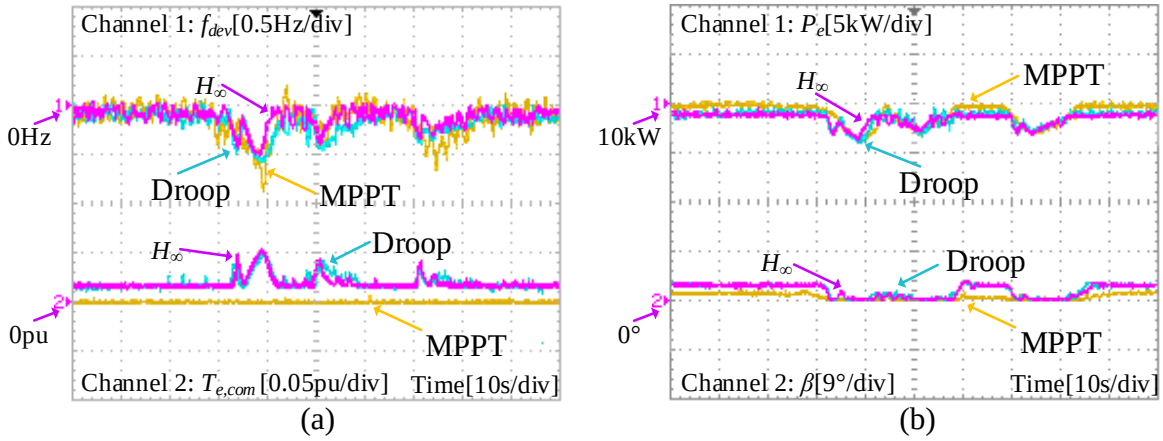

Figure 13. Experiment results when wind speed changes.

7. Conclusions

The gain scheduled control strategy based on H_∞ theory strategy in this paper enhances the frequency stability of isolated grid. Compared with other control methods, the torque compensation gain is further enhanced by the proposed strategy for the whole range of wind speeds. The proposed strategy nicely integrates the advantages of steady-state power reserves and inertia for regulating frequency, which enables achieving more power reserves with different deloading factors. The speed reference of pitch system is also improved to avoid decay of power compensation at over-rated wind speed. Various H_∞ control performance metrics including inhibiting frequency fluctuation, minimization of active power change, and smoothing power are confirmed by experiments. Comparing with the state-of-the-art MPPT and Droop methods, the frequency deviation with the proposed strategy is reduced by 0.16 Hz and 0.04 Hz, respectively, at over-rated wind speed, and 0.38 Hz and 0.06 Hz, respectively, when wind speed changes.

Author Contributions: All authors conceived and designed the study. H.W., Y.L. and Y.M. performed the simulation and wrote the manuscript with guidance from J.Y., Z.C. and S.H., W.G., G.Z. and L.Y. collaborated in the experiment verification and the analysis of results.

Funding: This research is supported by "Application Technology Research and Engineering Demonstration Program of National Energy" of China (NY20150303).

Conflicts of Interest: The authors declare no conflict of interest.

Appendix A

Table A1. Parameters of wind turbine.

c_1	0.5176	c_2	116	c_3	0.4	c_4	5
c_5	21	c_6	0.0068	A_r	20.1 m^2	k_{opt}	0.1767
k_{f1}	0.9	k_{f2}	0.8	ω_0	0.4	ω_1	0.97
$\omega_{r,\text{nom}}$	1	ω_2	1.02	ω_3	1.05	$\omega_{r,\text{max}}$	1.2

Table A2. Parameters of diesel generator.

R	0.08	K_I	7
T_d	0.005 s	T_g	0.1 s

Table A3. Parameters of system.

M	0.5	D	0.01

Table A4. Parameters at the operating point (V_w = 10 m/s).

ω_{r0}	34.2927 rad/s	a_1	0
a_2	78.4096	a_3	1979.1

Table A5. Parameters at the operating point (V_w = 13.5 m/s).

ω_{r0}	40.32 rad/s	a_1	−437.7964
a_2	101.5045	a_3	1696.9

References

1. Attya, A.B.; Dominguez-Garcia, J.L.; Anaya-Lara, O. A review on frequency support provision by wind power plants: Current and future challenges. *Renew. Sustain. Energy Rev.* **2018**, *81*, 2071–2087. [CrossRef]
2. Pradhan, C.; Bhende, C.N.; Samanta, A.K. Adaptive virtual inertia-based frequency regulation in wind power systems. *Renew. Energy* **2018**, *115*, 558–574. [CrossRef]
3. Attya, A.B.; Hartkopf, T. Wind turbine contribution in frequency drop mitigation—Modified operation and estimating released supportive energy. *IET Gener. Trans. Distrib.* **2014**, *8*, 862–872. [CrossRef]
4. Wu, Z.; Gao, W.; Gao, T.; Yan, W.; Zhang, H.; Yan, S.; Wang, X. State-of-the-art review on frequency response of wind power plants in power systems. *J. Mod. Power Syst. Clean Energy* **2018**, *6*, 1–16. [CrossRef]
5. Krpan, M.; Kuzle, I. Introducing low-order system frequency response modelling of a future power system with high penetration of wind power plants with frequency support capabilities. *IET Renew. Power Gener.* **2018**, in press. [CrossRef]
6. Bevrani, H.; Feizi, M.R.; Ataee, S. Robust frequency control in an islanded microgrid: H_∞ and μ-synthesis approaches. *IEEE Trans. Smart Grid* **2016**, *7*, 706–717. [CrossRef]
7. Wilches-Bernal, F.; Chow, J.H.; Sanchez-Gasca, J.J. A fundamental study of applying wind turbines for power system frequency control. *IEEE Trans. Power Syst.* **2016**, *31*, 1496–1505. [CrossRef]
8. Nguyen, N.; Mitra, J. An analysis of the effects and dependency of wind power penetration on system frequency regulation. *IEEE Trans. Sustain. Energy* **2016**, *7*, 354–363. [CrossRef]
9. Mitra, A.; Chatterjee, D. Active power control of DFIG-based wind farm for improvement of transient stability of power systems. *IEEE Trans. Power Syst.* **2016**, *31*, 82–93. [CrossRef]
10. Zoghlami, M.; Kadri, A.; Bacha, F. Analysis and application of the sliding mode control approach in the variable-wind speed conversion system for the utility of grid connection. *Energies* **2018**, *11*, 720. [CrossRef]

11. Martínez-Lucas, G.; Sarasúa, J.I.; Sánchez-Fernández, J.A. Frequency regulation of a hybrid wind–hydro power plant in an isolated power system. *Energies* **2018**, *11*. [CrossRef]
12. Rocabert, J.; Luna, A.; Blaabjerg, F.; Rodríguez, P. Control of power converters in AC microgrids. *IEEE Trans. Power Electron.* **2012**, *27*, 4734–4749. [CrossRef]
13. Wang, H.; Chen, Z.; Jiang, Q. Optimal control method for wind farm to support temporary primary frequency control with minimised wind energy cost. *IET Renew. Power Gener.* **2015**, *9*, 350–359. [CrossRef]
14. Ghosh, S.; Kamalasadan, S.; Senroy, N.; Enslin, J. Doubly fed induction generator (DFIG)-based wind farm control framework for primary frequency and inertial response application. *IEEE Trans. Power Syst.* **2016**, *31*, 1861–1871. [CrossRef]
15. Kamel, R.M.; Chaouachi, A.; Nagasaka, K. Three control strategies to improve the microgrid transient dynamic response during isolated mode: A comparative study. *IEEE Trans. Ind. Electron.* **2013**, *60*, 1314–1322. [CrossRef]
16. Pahasa, J.; Ngamroo, I. Coordinated control of wind turbine blade pitch angle and PHEVs using MPCs for load frequency control of microgrid. *IEEE Syst. J.* **2016**, *10*, 97–105. [CrossRef]
17. Hoseinzadeh, B.; Chen, Z. Intelligent load-frequency control contribution of wind turbine in power system stability. In Proceedings of the IEEE EUROCON, Zagreb, Croatia, 1–4 July 2013.
18. Asensio, A.P.; Gomez, S.A.; Rodriguez-Amenedo, J.L.; Plaza, M.G.; Carrasco, J.E.G.; de las Morenas, J.M.A.M. A voltage and frequency control strategy for stand-alone full converter wind energy conversion systems. *Energies* **2018**, *11*, 474. [CrossRef]
19. Xiong, L.; Li, Y.; Zhu, Y.; Yang, P.; Xu, Z. Coordinated control schemes of super-capacitor and kinetic energy of DFIG for system frequency support. *Energies* **2017**, *11*. [CrossRef]
20. Tang, Y.; Dai, J.; Ning, J.; Dang, J.; Li, Y.; Tian, X. An extended system frequency response model considering wind power participation in frequency regulation. *Energies* **2017**, *10*. [CrossRef]
21. Li, Y.; Xu, Z.; Wong, K.P. Advanced control strategies of PMSG-based wind turbines for system inertia support. *IEEE Trans. Power Syst.* **2017**, *32*, 3027–3037. [CrossRef]
22. Wu, Z.; Gao, W.; Wang, X.; Kang, M.; Hwang, M.; Kang, Y.C.; Gevogian, V.; Muljadi, E. Improved inertial control for permanent magnet synchronous generator wind turbine generators. *IET Renew. Power Gener.* **2016**, *10*, 1366–1373. [CrossRef]
23. Arani, M.F.M.; Mohamed, Y.A.R.I. Analysis and mitigation of undesirable impacts of implementing frequency support controllers in wind power generation. *IEEE Trans. Energy Convers.* **2016**, *31*, 174–186. [CrossRef]
24. Vidyanandan, K.V.; Senroy, N. Primary frequency regulation by deloaded wind turbines using variable droop. *IEEE Trans. Power Syst.* **2013**, *28*, 837–846. [CrossRef]
25. Moutis, P. Discussion on "primary frequency regulation by deloaded wind turbines using variable droop". *IEEE Trans. Power Syst.* **2014**, *29*, 414. [CrossRef]
26. Vidyanandan, K.V.; Senroy, N. Closure to discussion on "primary frequency regulation by deloaded wind turbines using variable droop". *IEEE Trans. Power Syst.* **2014**, *29*, 414–415. [CrossRef]
27. Arani, M.F.M.; Mohamed, Y.A.R.I. Analysis and impacts of implementing droop control in DFIG-based wind turbines on microgrid/weak-grid stability. *IEEE Trans. Power Syst.* **2015**, *30*, 385–396. [CrossRef]
28. Qin, Z.; Blaabjerg, F.; Loh, P.C. A rotating speed controller design method for power leveling by means of inertia energy in wind power systems. *IEEE Trans. Energy Convers.* **2015**, *30*, 1052–1060. [CrossRef]
29. Chen, Z.; Hu, Y. A hybrid generation system using variable speed wind turbines and diesel units. In Proceedings of the 29th Annual Conference of the IEEE Industrial Electronics Society, Roanoke, VA, USA, 2–6 November 2003.
30. Wang, Y.; Meng, J.; Zhang, X.; Xu, L. Control of PMSG-based wind turbines for system Inertial response and power oscillation damping. *IEEE Trans. Sustain. Energy* **2015**, *6*, 565–574. [CrossRef]
31. Wang, Y.; Bayem, H.; Giralt-Devant, M.; Silva, V.; Guillaud, X.; Francois, B. Methods for assessing available wind primary power reserve. *IEEE Trans. Sustain. Energy* **2015**, *6*, 272–280. [CrossRef]
32. Van, T.L.; Nguyen, T.H.; Lee, D.C. Advanced pitch angle control based on fuzzy logic for variable-speed wind turbine systems. *IEEE Trans. Energy Convers.* **2015**, *30*, 578–587. [CrossRef]
33. Fazeli, M.; Asher, G.M.; Klumpner, C.; Yao, L. Novel integration of DFIG-based wind generators within microgrids. *IEEE Trans. Energy Convers.* **2011**, *26*, 840–850. [CrossRef]

34. Zhong, Q.C.; Hornik, T. Cascaded current–voltage control to improve the power quality for a grid-connected inverter with a local load. *IEEE Trans. Ind. Electron.* **2013**, *60*, 1344–1355. [CrossRef]
35. Li, Y.W.; Vilathgamuwa, D.M.; Loh, P.C. Robust control scheme for a microgrid with PFC capacitor connected. *IEEE Trans. Ind. Appl.* **2007**, *43*, 1172–1182. [CrossRef]